crystals

MDPI

Article

Oxidized Graphite Nanocrystals for White Light Emission

Patrik Ščajev [1,*], Saulius Miasojedovas [1], Algirdas Mekys [1], Gediminas Kreiza [1], Justinas Čeponkus [2], Valdas Šablinskas [2], Tadas Malinauskas [1] and Arturs Medvids [3,*]

[1] Institute of Photonics and Nanotechnology, Faculty of Physics, Vilnius University, Saulėtekio Ave. 3, 10257 Vilnius, Lithuania; saulius.miasojedovas@ff.vu.lt (S.M.); algirdas.mekys@ff.vu.lt (A.M.); gediminas.kreiza@ff.vu.lt (G.K.); tadas.malinauskas@ff.vu.lt (T.M.)
[2] Institute of Chemical Physics, Faculty of Physics, Vilnius University, Saulėtekio Ave. 3, 10257 Vilnius, Lithuania; justinas.ceponkus@ff.vu.lt (J.Č.); valdas.sablinskas@ff.vu.lt (V.Š.)
[3] Institute of Technical Physics, Riga Technical University, Paula Valdena 3/7, LV 1048 Riga, Latvia
* Correspondence: patrik.scajev@ff.vu.lt (P.Š.); medvids@latnet.lv (A.M.)

Abstract: We investigated the formation of graphite nanocrystals covered with graphite oxide for white light generation. The nanoparticles were formed using cost-efficient oxidation of a carbon-based dye pigment at different temperatures and verified using X-ray diffraction and Raman measurements. Formation of the graphite nanoparticles via thermal annealing was observed, while their light emission increased at higher oxidation temperatures. This was associated with a higher amount of oxygen defect groups. The time-resolved photoluminescence measurements showed linearly faster decays at shorter wavelengths and similar decays at different annealing temperatures. Broadband and linear vs. excitation emission spectra of the particles were found to be suitable for white-light-emitting devices and phosphor markers. The fast photoluminescence decay opens the possibility for the application of nanoparticles in optical wireless communication technology.

Keywords: graphite; oxidation; nanocrystals; photoluminescence

Citation: Ščajev, P.; Miasojedovas, S.; Mekys, A.; Kreiza, G.; Čeponkus, J.; Šablinskas, V.; Malinauskas, T.; Medvids, A. Oxidized Graphite Nanocrystals for White Light Emission. *Crystals* **2024**, *14*, 505. https://doi.org/10.3390/cryst14060505

Academic Editor: Pavel Lukáč

Received: 26 April 2024
Revised: 19 May 2024
Accepted: 23 May 2024
Published: 25 May 2024

1. Introduction

Graphite is considered as the most stable form of carbon and can be found in various structures: amorphous, pyrolytic, crystalline flakes, nanoparticles, and fiber. The crystalline structure of graphite consists of layers of carbon atoms arranged in a hexagonal lattice [1]. Graphite nanoparticles have various properties, such as high surface area, due to their nanoscale dimensions, excellent heat and electrical conductivity [2], enhanced chemical and biological compatibility [1], corrosion resistance, and dimensional stability. Graphite nanoparticles are much cheaper than comparable oxide nanoparticles and metalloids. The lubrication properties and thermal conductivity of graphite are important for mechanical devices, while their recycling does not cause any pollution [3]. Graphite nanoparticles consist of π-electron-conjugated nanosized graphene sheets stacked on top of each other, with the peripheries surrounded by dangling bonds that react with species like oxygen and hydrogen, leading to a completely bound edge structure [4]. The existence of unbounded open edges around the graphite nanoparticle's peripheral region gives them a specific functionality that is absent in other carbon allotropes with closed surface systems, like carbon nanotubes and fullerene [5].

Typically, graphite nanoparticles are produced by graphitization of nanodiamond powder at high temperatures (1600 °C–2750 °C for an hour) in an inert atmosphere [5]. Graphite nanoparticles can also be synthesized via a chemical route in a low magnetic field by using a reaction between calcium citrate and nitric acid [6]. Graphite oxide (GO), also known as graphitic oxide, is a compound composed of carbon, oxygen, and hydrogen in varying ratios [7,8]. Graphite oxide is typically obtained by treating graphite with oxidizers and acids. Although it retains the layered structure of graphite, the spacing

between the layers becomes much larger and irregular. When dispersed in basic solutions or polar solvents, it yields monomolecular sheets known as graphene oxide (analogous to single-layer graphene) [6].

Applications of graphite and GO include micrometer-thick films of graphene oxide paper, also called graphite oxide membranes, which have been used to create strong paper-like materials, membranes, thin films, and composite materials [9]. Unique GO properties, such as its dielectric behavior, find applications in memristors and multipolar electrodes for lithium-ion batteries [10]. The nanoparticles can also be used in lubrication agents, composites [11], biosensors [12], fuel cells [13], supercapacitor batteries [14], and transistors [15].

Graphite oxide consists of stacked graphene oxide monolayers. Graphene oxide is an excellent two-dimensional candidate for photoluminescent material because of its unique optical properties compared to pure graphene [16]. The existence of an internal band gap in graphene oxide enriches its optical properties significantly [17]. Therefore, it has been widely applied in many fields such as material science, biomedicine, anti-counterfeiting, and so on. Over the past decade, it has attracted the attention of many researchers as a luminescent material, but its luminescence mechanism is still ambiguous, although some theoretical explanations have been proposed. In addition, it has fluorescence quenching properties, which can be used in medical imaging and biosensors [18]. On the other hand, the time-resolved PL decay properties of three-dimensional GO or oxidized graphite have not been investigated sufficiently.

In this work, we present a cost-efficient method for the preparation of nanographite crystals covered with graphite oxide to obtain broadband light emitters and investigate their temporal photoluminescence emission properties.

2. Materials and Methods

The nanoparticle layers were prepared by spay-coating polished silicon substrates [19] using a precursor of colloidal graphite (MIL-L-24131C) in isopropanol. A spray gun with propane was used to coat the layers. The layers were annealed in hot air at 200 °C (S1) and 300 °C (S2) temperatures. For comparison, an unannealed sample was also studied to show the absence of nanoparticles. We used silicon substrate as it is a cheap and common electronic material [20] on which the nanoparticle emitters can be integrated to obtain light-emitting devices compatible with silicon electronics.

Crystalline properties of the particles were investigated using grazing incidence X-ray diffraction (GIXRD) measurements using Cu Kα radiation from a 9 kW X-ray tube with a rotating anode (SmartLab, Rigaku, Tokyo, Japan) [21]. The absorption spectra were measured using a Perkin Elmer Lambda 950 UV-NIR absorption spectrometer. For this purpose, the sample layers were mechanically grounded and dispersed onto quart plates. The absorbance spectra were corrected by subtracting the quartz plate absorbance spectra. For Raman spectra acquisition, a Confocal Raman Grating Spectrometer with a microscope "MonoVista CRS" (S&I GmbH, Warstein, Germany) was used. AFM scans were performed using the Bruker Dimension Icon microscope. SEM scans were performed using Hitachi SU8230. Time-resolved photoluminescence (TRPL) measurements were performed in a standard back-scattering geometry using a Hamamatsu streak camera (C10627) attached to an Acton monochromator (30 cm focal length, ~5 nm spectral resolution) [22]. For excitation, 180 fs pulses with a repetition rate of 10 kHz from an ORPHEUS parametric amplifier, pumped by a PHAROS laser, were used. The 320 nm wavelength (~0.5 nm linewidth) was used for excitation of the studied nanoparticle layers. An excitation spot diameter of 350 μm was used. The excitation intensity was regulated by two continuously variable neutral density filters (NDC-50C-2). For scattered excitation light-blocking, we placed a longpass filter with a cut-off wavelength of 340 nm before the monochromator input slit.

3. Results and Discussion

Figure 1 shows optical microscope images of the samples. Sample S1 is macroscopically not continuous, while S2 has much better coverage (the blue color in Figure 1a is due to the reflection from the silicon substrate). On a smaller scale, AFM and SEM scans (Figure 2) also show better nanograin coalescence and a smoother surface in sample S2, indicating that annealing at 300 °C is more favorable for the production of the nanographite layer. AFM layer roughness was 228 nm and 159 nm for S1 and S2, respectively. In the SEM images (Figure 2c,d), the graphite platelets are clearly observable.

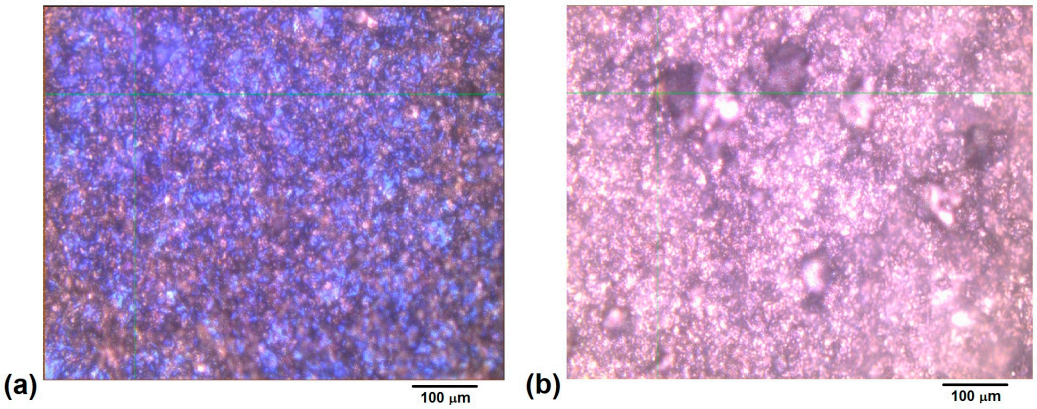

Figure 1. Optical microscope images of S1 (**a**) and S2 (**b**).

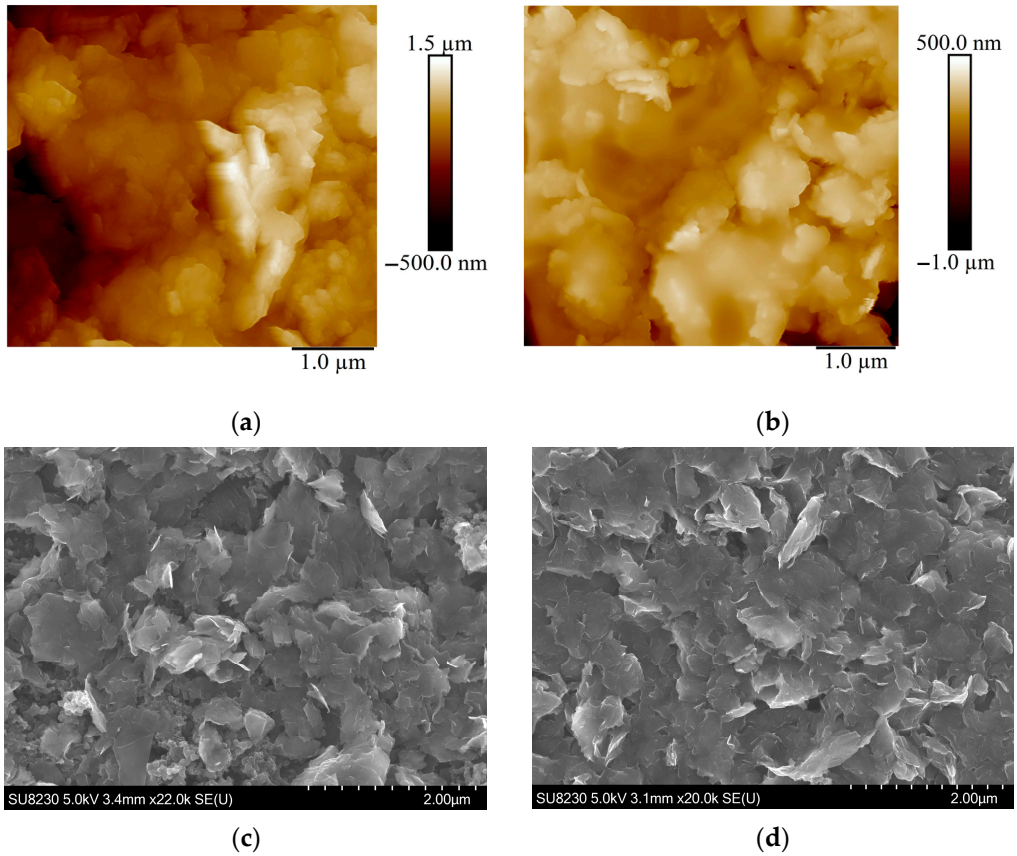

Figure 2. AFM images of the S1 (**a**) and S2 (**b**) samples. SEM images of the S1 (**c**) and S2 (**d**) samples.

Figure 3a shows the GIXRD scans ranging from 2θ = 20 to 70 deg for the two samples. Two peaks at 2θ = 26.4 deg and 2θ = 44.5 deg are observed in both samples. These two peaks correspond to the most intense (002) and (101) reflections of graphite according to the PDF card No.: 01-084-9339. Using the Scherrer equation and assuming that the broadening of the XRD peaks is solely due to the finite size of the crystallites, we deduced that the lower limit of the graphite crystallite size (plate thickness) is around 14 nm in both samples. The graphite oxide peaks were not observed. Graphite inter-plane distance is 0.335 nm; thus, the particles consist of around 42 graphene layers. The absorbance spectra are provided in Figure 3b. The absorbance of S1 reduces at a shorter wavelength, which is typical for graphite. On the other hand, for S2, the absorbance is weakly dependent on the wavelength, which can be explained by strong additional graphite oxide absorption due to the higher oxidation temperature used during S2 preparation. Graphite (G) and graphite oxide (GO) absorption contributions from [23] are shown in Figure 3b for comparison. A similar situation was observed in multilayer graphene, where absorption decreases weakly at shorter wavelengths, while in graphene oxide the absorption increases strongly at wavelengths shorter than 400 nm [24,25]. This is a direct consequence of graphene (graphite) having a much lower bandgap compared with graphene (graphite) oxide.

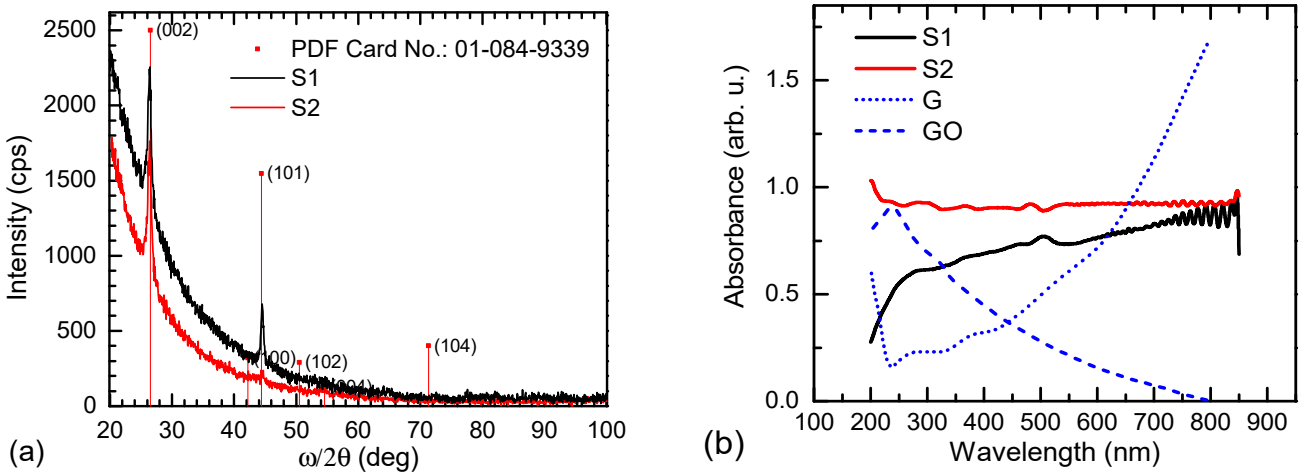

Figure 3. (**a**) GIXRD patterns of S1 and S2 samples. Diffraction peaks were identified according to the PDF Card of graphite No.: 01-084-9339. (**b**) Absorbance spectra of the S1 and S2 samples. Graphite oxide (GO) and graphite (G) absorbances are taken from [23].

The Raman spectra are provided in Figure 4. Again, S2 shows the best properties, as evidenced by the absence of the Si peaks observed in S1. The Si peaks are present due to the large holes in the S1 layer formed after annealing (see Figure 1). In the initial non-annealed layer, the Si peaks are almost absent due to the continuous coverage of the substrate by precursor solution. Additionally, no graphite peaks were observed. D and G bands are indicated on the plots. Graphite has a very weak D band in comparison to the G band. The observed spectra are a signature of GO, in which similar D and G relative peak amplitudes and positions have been determined [26,27]. As the GIXRD patterns (Figure 3a) do not show GO, this discrepancy indicates that GO either constitutes only a small fraction of the volume of graphite nanoparticles or the formed graphite oxide is amorphous [28].

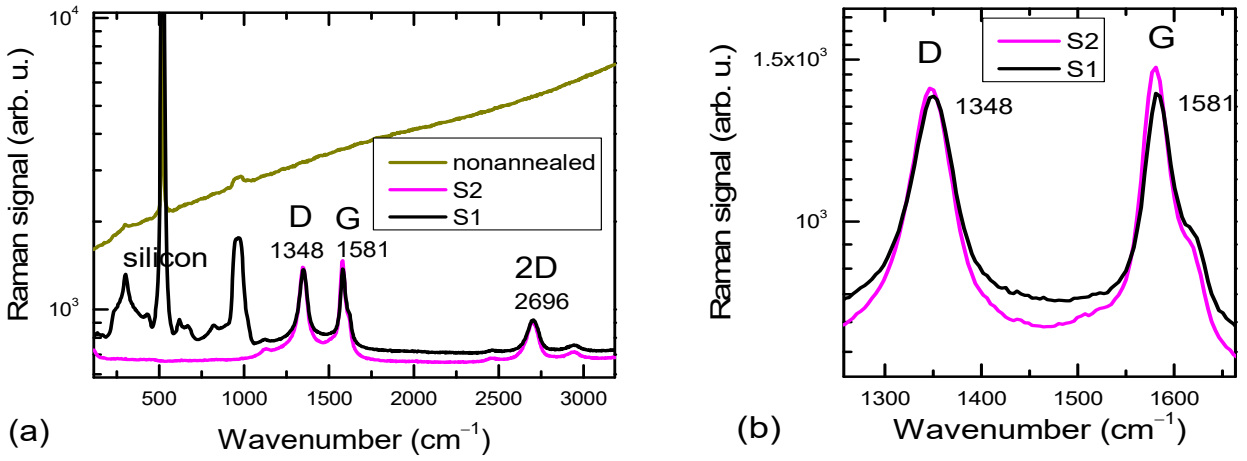

Figure 4. Raman spectra of the studied samples. Main graphite/GO peak positions are indicated (**a**). Magnified region (**b**).

The photoluminescence spectra of the studied layers are provided in Figure 5. S2 has a magnitude stronger emission that can be explained by better surface coverage and better grain coalescence (Figure 2), leading to stronger exciton emission due to a lower defect density. The peak around 360 nm corresponds to a π–π* transition [16]. Broad long wavelength PL tail can be correlated to the presence of localized states on the oxygen groups denoted as band 1 (~400 nm) and band 2 (~550 nm) [16]. The π–π* transition in S2 is almost invisible, indicating more efficient photo-excited exciton transfer to the oxygen defect groups and their further efficient radiative emission [16]. Three kinds of functionalized groups, C-O, C=O, and O=C-OH, are involved in the fluorescence of graphene oxide [27]. The broadness of the PL peak is due to varying oxygen concentrations, leading to a high variety of emitting defects. The latter is enhanced by higher oxidation temperatures, leading to the possibility of more efficient white light emission. In S2, the spectra change weakly with excitation by blue-shifting, indicating saturation of the lowest localization levels. Additionally, a higher annealing temperature leads to stronger oxidation and a thicker graphene oxide layer on the particles, leading to a stronger luminescence. More oxygen explains larger bandgap emission of the graphene oxide, verifying known data showing that the GO bandgap increases from 1 eV to 3 eV for a 10–50% O/C ratio increase [29]. This also explains the blue shift of the S2 PL spectrum with respect to S1 (maximum shifts from 450 nm to 420 nm). Transfer of the higher energy less localized excitons to the nonradiative defects is faster.

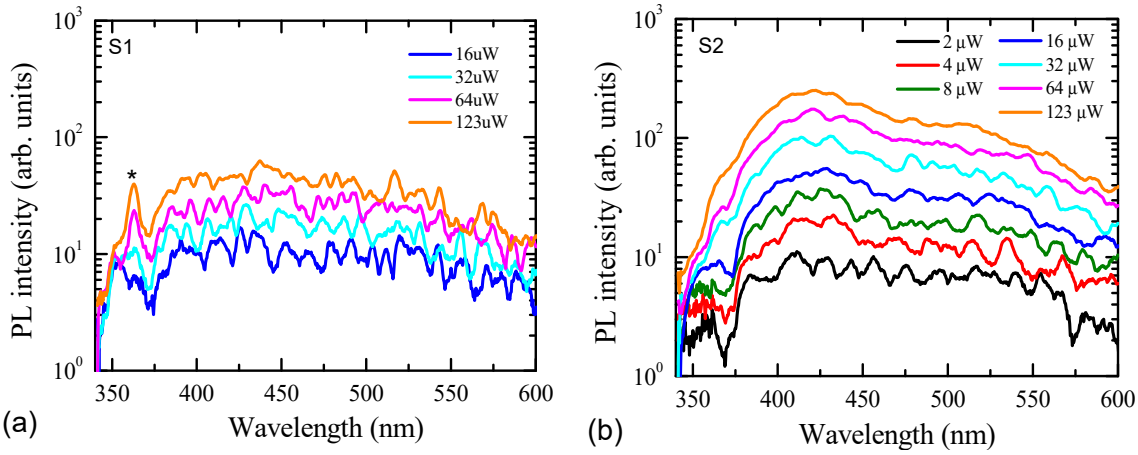

Figure 5. Photoluminescence spectra of the S1 (**a**) and S2 (**b**) samples at variable excitations in 10 ns time windows.

The spectrum of the emitters has good white light quality properties, providing a color rendering index (CRI) of 85, which would be suitable for white-light-emitting devices.

The PL decay shapes were similar at variable excitations; thus, we plotted the PL decays at the highest excitation in Figure 6. The decays at different emission wavelengths were found to be different. Stretch exponential functions were fitted to the decays. The stretch exponent $I_{PL} = I_0 \exp(-(t/\tau)^{\beta})$ was used as a fitting formula for the PL decays in Figure 6; the corresponding fitting parameters are also shown in Figure 6. The lifetime τ dependence on the wavelength in both samples is provided in Figure 7b. A short wavelength range corresponds to faster decay, which can be explained by less localized high-energy excitons that can more easily reach the non-radiative defects on the grain boundaries and exciton thermalization. Stretching is caused by different interface recombination rates of different particles. Decay times are similar in both samples, indicating that thicker graphite oxide may be formed with similar emissive properties. The fast sub-nanosecond PL decays show a possibility of using these emitters for optical wireless communication technology (LIFI) [30].

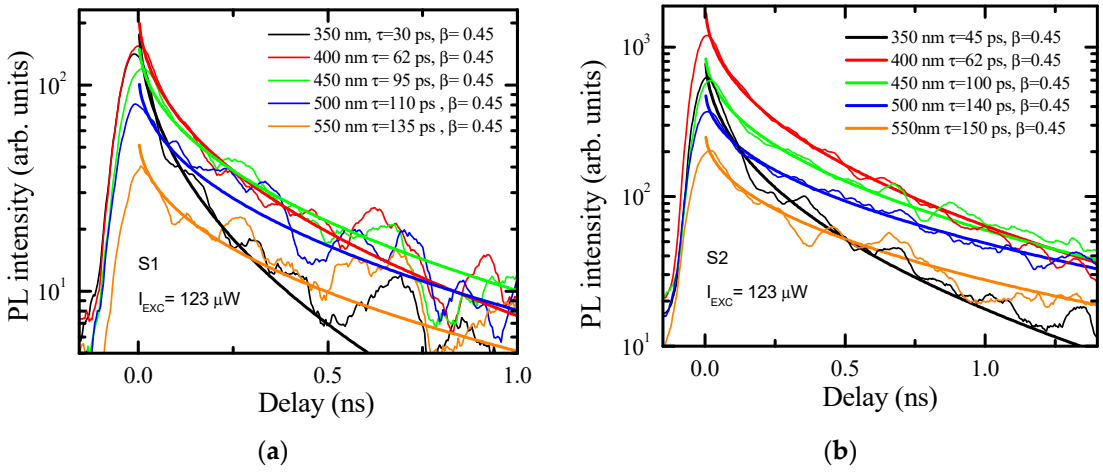

Figure 6. Photoluminescence decays of S1 (**a**) and S2 (**b**) samples at different emission wavelengths. The solid lines are stretch exponential fits, with parameters provided on the plots.

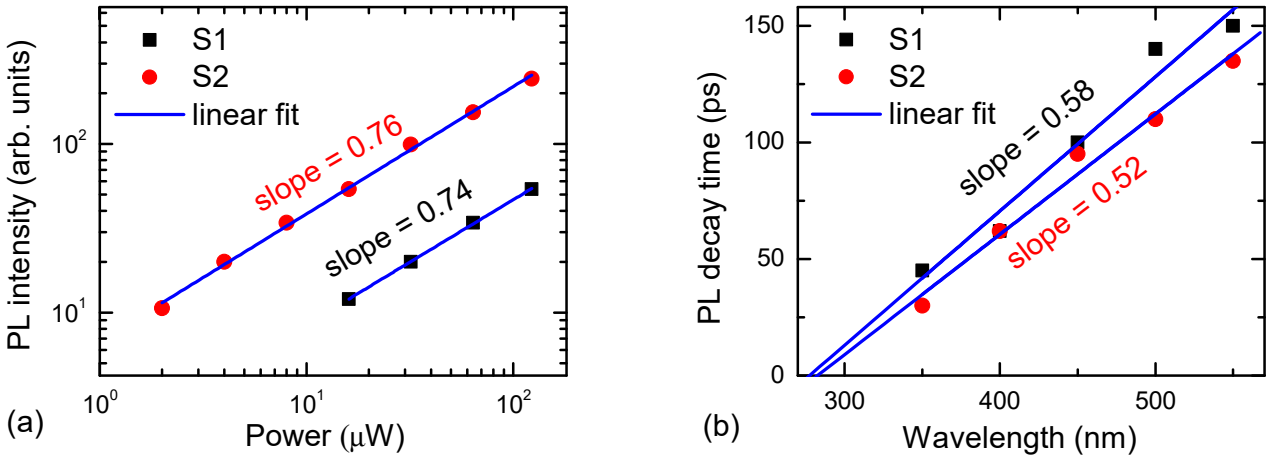

Figure 7. PL intensity excitation dependences (**a**) and PL decay time emission wavelength dependences (**b**).

The PL intensity vs. excitation slope is close to unity, indicating a small saturation of the excitons localized on the oxygen defects (Figure 7a). Sample 1 has similar spectra and decays but almost an order of magnitude weaker PL emission—it correlates with weaker oxidation

(Figure 3b) and poorer crystallite coalescence (Figures 1 and 2). The spaces between the crystallites can work as nonradiative surface defects [31], leading to PL quenching. The PL decay time in Figure 7b has linear wavelength dependence in both samples, indicating a universal dependence for both layers irrespective of their emission intensity. The lifetime dependences vs. wavelength were fitted as $\tau_{PL1} = 0.58$ ps/nm $\times$ (λ(nm) $-$ 275 nm) and $\tau_{PL1} = 0.52$ ps/nm $\times$ (λ(nm) $-$ 281 nm) for S1 and S2, respectively. These dependences could be explained by the exciton decay limited by the thermalization in the oxygen-group defects in both samples and the cutoff wavelength of 275–281 nm (4.4 eV) can, approximately, correspond to the graphene oxide σ band with the highest energy (4.2 eV [16]). Further research is needed to obtain more efficient oxidized graphite nanoparticles for white light emitters.

4. Conclusions

We obtained graphite nanoparticles covered with graphite oxide by using a cost-efficient method of thermal annealing of a carbon-based dye. The 300 °C annealing temperature was found to be optimal for obtaining the best morphology and the maximum luminescence intensity in the graphite nanoparticles. The emission was described by a stretch exponential function with linearly faster decay times at shorter wavelengths due to the less delocalized excitons. The nanoparticle white emission spectrum has a high color rendering index CRI of 85, which would be suitable for white-light-emitting devices, whereas the fast PL decays show the possibility of using these emitters for LIFI optical wireless communication technology.

Author Contributions: Conceptualization, A.M. (Arturs Medvids); methodology, P.Š., S.M., A.M. (Algirdas Mekys), G.K., J.Č., V.Š. and T.M.; investigation, P.Š., S.M., A.M. (Algirdas Mekys), G.K., J.Č., V.Š., T.M. and A.M. (Arturs Medvids); data curation, P.Š., S.M., A.M. (Algirdas Mekys), G.K., J.Č., V.Š. and T.M.; writing—original draft preparation, P.Š.; writing—review and editing, P.Š.; project administration, P.Š. and A.M. (Arturs Medvids). All authors have read and agreed to the published version of the manuscript.

Funding: This research was funded by the COST action: "European Network for Innovative and Advanced Epitaxy" (CA20116, P-COST-21-6, 2021–2025).

Data Availability Statement: The data that support the findings of this study are available upon reasonable request from the authors.

Conflicts of Interest: The authors declare no conflicts of interest.

References

1. Li, J.; Zeng, H.; Zeng, Z.; Zeng, Y.; Xie, T. Promising Graphene-Based Nanomaterials and Their Biomedical Applications and Potential Risks: A Comprehensive Review. *ACS Biomater. Sci. Eng.* **2021**, *7*, 5363–5396. [CrossRef]
2. Xie, Y.; Wang, X. Thermal conductivity of carbon-based nanomaterials: Deep understanding of the structural effects. *Green Carbon* **2023**, *1*, 47–57. [CrossRef]
3. Zhu, H.; Zhang, C.; Tang, Y.; Wang, J.; Ren, B.; Yin, Y. Preparation and thermal conductivity of suspensions of graphite nanoparticles. *Carbon* **2007**, *45*, 226–228. [CrossRef]
4. Rasuli, H.; Rasuli, R. Nanoparticle-decorated graphene/graphene oxide: Synthesis, properties and applications. *J. Mater. Sci.* **2023**, *58*, 2971–2992. [CrossRef]
5. Brassett, A.J.; Friend, R.H.; Hale, R.D.; Marvin, D.A.; Perham, R.N. Structure and electronic properties of inovirus. *Synth. Met.* **1991**, *41*, 189–192. [CrossRef]
6. Krishna, B.G.; Rao, M.J. Chemical synthesis of graphite nanoparticles and study of microwave radiation absorption by graphite nanocomposites. *Int. J. Adv. Res.* **2015**, *3*, 391–397.
7. Shen, L.; Zhang, L.; Wang, K.; Miao, L.; Lan, Q.; Jiang, K.; Lu, H.; Li, M.; Li, Y.; Shen, B.; et al. Analysis of oxidation degree of graphite oxide and chemical structure of corresponding reduced graphite oxide by selecting different-sized original graphite. *RSC Adv.* **2018**, *8*, 17209. [CrossRef] [PubMed]
8. Chetibi, L.; Hamana, D.; Silvan, M.M.; Achour, S. Electrochemical synthesis and characterization of graphite nanoparticles. *Appl. Phys. A* **2022**, *128*, 578. [CrossRef]
9. Mohan, V.B.; Lau, K.; Hui, D.; Bhattacharyya, D. Graphene-based materials and their composites: A review on production, applications and product limitations. *Compos. Part B Eng.* **2018**, *142*, 200–220. [CrossRef]

10. Sundar, L.S.; Mir, M.A.; Ashraf, M.W.; Djavanroodi, F. Synthesis and characterization of graphene and its composites for Lithium-Ion battery applications: A comprehensive review. *Alex. Eng. J.* **2023**, *78*, 224–245. [CrossRef]
11. Petit, C.; Bandosz, T.J. MOF–Graphite Oxide Composites: Combining the Uniqueness of Graphene Layers and Metal–Organic Frameworks. *Adv. Mater.* **2009**, *21*, 4753–4757. [CrossRef]
12. Kitko, K.E.; Zhang, Q. Graphene-Based Nanomaterials: From Production to Integration With Modern Tools in Neuroscience. *Front. Syst. Neurosci.* **2019**, *13*, 26. [CrossRef] [PubMed]
13. Farooqui, U.R.; Ahmad, A.L.; Hamid, N.A. Graphene oxide: A promising membrane material for fuel cells. *Renew. Sustain. Energy Rev.* **2018**, *82*, 714–733. [CrossRef]
14. Arsha, M.S.; Biju, V. Can graphite oxide active material achieve commercial supercapacitor level energy and power densities? Binder free coating and WIS electrolyte strategies. *J. Energy Storage* **2023**, *70*, 108064. [CrossRef]
15. Standley, B.; Mendez, A.; Schmidgall, E.; Bockrath, M. Graphene–Graphite Oxide Field-Effect Transistors. *Nano Lett.* **2012**, *12*, 1165–1169. [CrossRef] [PubMed]
16. Liang, H.F.; Smith, C.T.G.; Mills, C.A.; Silva, S.R.P. The band structure of graphene oxide examined using photoluminescence spectroscopy. *J. Mater. Chem. C* **2015**, *3*, 12484. [CrossRef]
17. Xiao, X.; Zhang, Y.; Zhou, L.; Li, B.; Gu, L. Photoluminescence and Fluorescence Quenching of Graphene Oxide: A Review. *Nanomaterials* **2022**, *12*, 2444. [CrossRef] [PubMed]
18. Sun, X.; Liu, Z.; Welsher, K.; Robinson, J.T.; Goodwin, A.; Zaric, S.; Dai, H. Nano-Graphene Oxide for Cellular Imaging and Drug Delivery. *Nano Res.* **2008**, *1*, 203–212. [CrossRef] [PubMed]
19. Ščajev, P.; Malinauskas, T.; Seniutinas, G.; Arnold, M.D.; Gentle, A.; Aharonovich, I.; Gervinskas, G.; Michaux, P.; Hartley, J.; Mayes, E.; et al. Light-induced reflectivity transients in black-Si nanoneedles. *Sol. Energy Mater. Sol. Cells* **2016**, *144*, 221–227. [CrossRef]
20. Akinwande, D.; Huyghebaert, C.; Wang, C.-H.; Serna, M.I.; Goossens, S.; Li, L.-J.; Wong, H.-S.P.; Koppens, F.H.L. Graphene and two-dimensional materials for silicon technology. *Nature* **2019**, *573*, 507–518. [CrossRef]
21. Ščajev, P.; Durena, R.; Onufrijevs, P.; Miasojedovas, S.; Malinauskas, T.; Stanionyte, S.; Zarkov, A.; Zukuls, A.; Bite, I.; Smits, K. Morphological and optical property study of Li doped ZnO produced by microwave-assisted solvothermal synthesis. *Mater. Sci. Semicond. Proc.* **2021**, *135*, 106069. [CrossRef]
22. Carra, C.; Medvids, A.; Litvinas, D.; Ščajev, P.; Malinauskas, T.; Selskis, A.; Roman, H.E.; Bazaka, K.; Levchenko, I.; Riccardi, C. Hierarchical Carbon Nano-Silica Metamaterials: Implications for White Light Photoluminescence. *ACS Appl. Nano Mater.* **2022**, *5*, 4787–4800. [CrossRef] [PubMed]
23. Fauzi, F.; Azizi, F.; Musawwa, M.M.; Dwandaru, W.S.B. Synthesis and Characterisations of Reduced Graphene Oxide Prepared by Microwave Irradiation with Sonication. *J. Phys. Sci.* **2021**, *32*, 1–13. [CrossRef]
24. Johra, F.T.; Lee, J.-W.; Jung, W.-G. Facile and safe graphene preparation on solution based platform. *J. Ind. Eng. Chem.* **2014**, *20*, 2883–2887. [CrossRef]
25. Umar, I.M.A.; Yap, C.C.; Awang, R.; Salleh, M.M. Effect of thermal reduction temperature on the optical and electrical properties of multilayer graphene. *J. Mater. Sci. Mater. Electron.* **2017**, *28*, 1038–1041. [CrossRef]
26. Perumbilavil, S.; Sankar, P.; Rose, T.P.; Philip, R. White light Z-scan measurements of ultrafast optical nonlinearity in reduced graphene oxide nanosheets in the 400–700 nm region. *Appl. Phys. Lett.* **2015**, *107*, 051104. [CrossRef]
27. Shang, J.; Ma, L.; Li, J.; Ai, W.; Yu, T.; Gurzadyan, G.G. The Origin of Fluorescence from Graphene Oxide. *Sci. Rep.* **2012**, *2*, 792. [CrossRef] [PubMed]
28. Liu, L.; Wang, L.; Gao, J.; Zhao, J.; Gao, X.; Chen, Z. Amorphous structural models for graphene oxides. *Carbon* **2012**, *50*, 1690–1698. [CrossRef]
29. Mei, Q.; Liu, B.; Han, G.; Liu, R.; Han, M.-Y.; Zhang, Z. Graphene Oxide: From Tunable Structures to Diverse Luminescence Behaviors. *Adv. Sci.* **2019**, *6*, 1900855. [CrossRef] [PubMed]
30. Subha, T.D.; Subash, T.D.; Rani, N.E.; Janani, P. Li-Fi: A Revolution in Wireless Networking. *Mater. Today Proc.* **2020**, *24*, 2403–2413. [CrossRef]
31. Mondal, S.; Ghosh, S. Quantifying defects in graphene oxide structures. *Carbon Trends* **2024**, *14*, 100323. [CrossRef]